December 1981 LRP 189/81

RADIAL STRUCTURE OF INTERNAL UNSTABLE IDEAL MHD MODES IN THE RANGE OF INTERMEDIATE TOROIDAL WAVE NUMBERS

R. Gruber, F. Troyon and T. Tsunematsu

RADIAL STRUCTURE OF INTERNAL UNSTABLE IDEAL MHD MODES IN THE RANGE OF INTERMEDIATE TOROIDAL WAVE NUMBERS

R. Gruber, F. Troyon and T. Tsunematsu*
Centre de Recherches en Physique des Plasmas
Association Euratom - Confédération Suisse
Ecole Polytechnique Fédérale de Lausanne
CH-1007 Lausanne / Switzerland

ABSTRACT

By extracting the ballooning phase factor from the displacement vector, the most unstable modes of the internal ideal MHD spectrum of two families of JET-like Tokamak configurations (with high shear and with low shear) can be calculated with a spectral code over a wide range of values of the toroidal wave number n. In the range of intermediate n-numbers ($3 \leq n \leq 100$), we present the radial and azimuthal structures of the amplitude of the displacement and the corresponding potential energy distribution. The eigensolutions behave qualitatively as expected from the ballooning mode theory.

---

* present address: JAERI, Tokai-Mura, Japan

1. INTRODUCTION

Recently there has been a lively interest in the spectrum of internal modes of axisymmetric toroidal plasmas. Extensions to the ballooning mode theory (Connor et al., 1978) are still being considered in order to increase its range of applicability to low shear (Hastie and Taylor, 1981) and lower toroidal wavenumber n (Charlton et al., 1980; Dewar et al., 1981; Hastie and Taylor, 1981; Takeda et al., 1981).

Standard spectral codes (Grimm et al., 1975; Gruber et al., 1981a) provide information for the lowest values of n. However, there remains a sizable gap in the intermediate range of n for which the modes exhibit some features of a ballooning mode while still involving all, or a large fraction, of the plasma. In practice, the largest value of toroidal wavenumber that can be handled with the published version of ERATO (Gruber et al., 1981a) is given approximately by $nq_{max} \leq 10$. This limit is due to the difficulty in reproducing numerically the fast angular variation of the mode (since it is very expensive with respect to computing time). Extracting from the eigenvector the fast varying ballooning phase factor (see Gruber et al., 1981b), the angular dependence of the amplitude is given, for all values of n, by the angular variation of the equilibrium quantities. In general, there remains a fast radial variation due to the many singular surfaces within the plasma. With this new code we can now study a much wider range of n values, which is expected to overlap the range of applicability of the ballooning codes.

In this paper we present the results of calculations using this new code which investigates the transition from the low-n global modes

to the high-n localized ballooning modes for two families of Tokamak equilibria. Realizing from the theory of ballooning modes that shear is a crucial parameter, we have chosen one family with high shear and the other with low shear. Both have been already studied in some detail for low-n modes (Berger et al., 1980; Gruber et al., 1979) and in the limit n = ∞ (Sykes et al., 1979; Rousset et al., 1979), so that some points of reference are available.

2. THE EQUILIBRIA

An axisymmetric toroidal equilibrium is described in cylindrical coordinates r,z,ϕ by the well-known Grad-Shafranov equation for the magnetic flux $\psi(r,z)$

$$r\frac{\partial}{\partial r}\left(\frac{1}{r}\frac{\partial\psi}{\partial r}\right)+\frac{\partial^2\psi}{\partial z^2}=-rJ_\phi\equiv-r^2\frac{dp}{d\psi}-T\frac{dT}{d\psi}, \quad (1)$$

where $p(\psi)$ is the plasma pressure, $T(\psi)\equiv rB_\phi$ the toroidal flux, B_ϕ the toroidal magnetic field and J_ϕ the toroidal current density. The normalization is chosen such that $\psi = 0$ on the magnetic axis. We shall only consider equilibria having an up-down reflection symmetry.

A poloidal-like angle, χ, is constructed according to $d\chi = Td\ell/qr^2B_p$, where $d\ell$ is the differential distance along a meridian cross-section, q is the safety factor and $B_p \equiv |\underline{\nabla}\psi|/r$ is is the poloidal field. The origin of χ is chosen to lie on the outer plane of symmetry, $z = 0, r > R_m$ (where R_m is the radius of the magnetic axis), and χ varies from $-\pi$ to $+\pi$ (Fig. 1).

We consider two families of JET-like equilibria. The first (labeled W) was proposed by Sykes et al. (1977). Its source functions are given by

$$\frac{dp}{d\psi} = \sigma\left(0.894\,\frac{\tilde{\psi}}{\sigma} - 1.833\,\frac{\tilde{\psi}^2}{\sigma^2}\right),$$
$$T\,\frac{dT}{d\psi} = \sigma\left(1.833\,R_m^2\,\frac{\tilde{\psi}^2}{\sigma^2} + 40.2\,\frac{\tilde{\psi}^4}{\sigma^4}\right), \qquad (2)$$

where $\tilde{\psi} = \psi - \psi_s$ and ψ_s is the flux at the surface with the boundary condition $T = 1$ at the surface. There is only one free parameter, σ, the so-called Oak-Ridge scaling parameter. Changing the value of σ does not change the magnetic field topology. Designating by the index 1 the values of quantities for $\sigma = 1$, the dependence on σ of the most important quantities is

$$p = \sigma^2 p_1\,, \quad T^2 = 1 + \sigma^2(T_1^2 - 1)$$
$$I = \sigma I_1\,, \quad q = \frac{T}{T_1}\,\frac{q_1}{\sigma} \approx \frac{q_1}{\sigma}\,, \quad \beta_I \equiv \frac{8\pi\iint p\,d^2x}{\mu_0 I^2} = \beta_{I_1}\,, \qquad (3)$$

when I denotes the total toroidal current defined by

$$I = \iint J_\phi\,d^2x\,. \qquad (4)$$

The scaling allows the possibility of varing β, while keeping $\beta_I = 2.13$ constant. This family of equilibria has been studied extensively in the past with the tools then available (Gruber et al., 1979; Sykes et al., 1979).

The second family is a particular subset of Solovev equilibria (Solovev, 1968; Küppers et al, 1971) characterised by its source functions

$$\frac{dp}{d\psi} = -\sigma \quad , \quad T\frac{dT}{d\psi} = 0 \, , \tag{5}$$

and the shape of the plasma surface

$$z^2 r^2 + \left(r^2 - 1\right)^2 = 0.25 \, . \tag{6}$$

The surface is D-shaped with an aspect ratio of 3 and an elongation of 2. The scaling factor again provides for control over the total current while keeping $\beta_I \approx .90$ constant.

Graphs of q/q_{axis} versus $s = \sqrt{\psi}/\psi_s$ are shown, for the two families of equilibria, in Fig. 2. The equilibria denoted by W6 have high shear and high β_I, while the Solovev equilibria, denoted by S1, have low shear and moderate β_I.

3. EXTRACTION OF THE BALLOONING PHASE FACTOR

Around the marginal point of the linear ideal MHD operator, the poloidal (χ direction) variation of an unstable displacement $\underline{\xi}$ is given essentially by

$$\frac{\partial \xi}{\partial \chi} + in q \xi \cong 0 \, . \tag{7}$$

This fact suggests a variable transformation

$$\underline{\xi} = \hat{\underline{\xi}}\, e^{-inq\chi} , \tag{8}$$

leading to

$$\frac{\partial \underline{\xi}}{\partial \chi} + inq\,\underline{\xi} = \frac{\partial \hat{\underline{\xi}}}{\partial \chi} . \tag{9}$$

The transformed displacement $\hat{\underline{\xi}}$ with its components $\hat{X}$, $\hat{V}$ and $\hat{Y}$ (in the radial, poloidal and toroidal direction, respectively) only contains the amplitude of the oscillating function $\underline{\xi}$. The up-down symmetry condition at $\chi = \pi$

$$\underline{\xi}(\pi+\varepsilon) = \underline{\xi}^{*}(\pi-\varepsilon) \tag{10}$$

which was imposed in the original ERATO code (Gruber et al., 1981a), now becomes

$$\hat{\underline{\xi}}(\pi+\varepsilon)\, e^{-inq(\pi+\varepsilon)} = \hat{\underline{\xi}}^{*}(\pi-\varepsilon)\, e^{+inq(\pi-\varepsilon)} \tag{11}$$

The procedure for including this symmetry condition in the ERATO code is described in detail by Gruber et al. (1981b).

4. INTERNAL STABILITY OF HIGH β_p, HIGH SHEAR, JET-SHAPED PLASMA EQUILIBRIA

In a search for high-β stable equilibria, Sykes et al. (1977) considered an interesting class of JET-shaped equilibria. The stability of these equilibria was subsequently examined in great detail in the low-n region (Gruber et al., 1979) and in the ballooning limit (Sykes et al., 1979). Stability was found with a conducting wall at the boundary of the plasma, both for low-n modes and in the ballooning limit, up to a maximum value of β. This β limit was found to be roughly the same for each value of n studied, n = 1, 2 and 3, but substantially higher than the value given by the ballooning limit. The important question of the transition between the low-n and the ballooning limit was beyond reach so that the relevance of the ballooning limit could not be assessed. It was noted, however, that above the instability threshold, the most unstable mode, for each value of n, exhibits strong ballooning on the outside of the torus. This last feature suggests that a code in which the ballooning phase factor is extracted (Gruber et al., 1981a; 1981b) is well suited to study the stability of these equilibra.

In Fig. 3 is plotted, for different toroidal mode numbers, n, the square of the growthrate, Γ^2, versus the safety factor on axis, q_0. For a given value of q_0, the growthrate increases monotonically with mode number. Increasing q_0, the low-n modes are stabilized first. The extrapolated curve for $n = \infty$ fits the analytic stability limit of the ballooning theory for $\Gamma^2 = 0$. The stability limit given by the ballooning theory is formulated for infinitely small wavelengths. We know, however, that for this case MHD is no longer valid. Introducing finite Larmor radius effects, which is often referred to as "ω^* stabi-

lization" (Itoh and Itoh, 1981), one finds that the n = 100 curve is stabilized by kinetic effects for $q_0 > 2.15$. This means that the "realistic" high-n stability limit is not at $q_0 = 2.4$ but at $q_0 = 2.15$, which corresponds to an increase of β from 4.8% to 5.7%.

In Fig. 4 are shown the azimuthal and radial profiles of the eigenmode amplitude for different values of n. The azimuthal profile of the radial displacement, $X(\chi)$, is shown for the magnetic surface on which the potential energy density is a minimum. The position of this magnetic surface is different for different values of n. For the representation of the radial structure, we fix $\chi = 0$. The safety factor was chosen to be $q_0 = 1.09$ which guarantees a strong ballooning mode. As predicted by the ballooning theory, the amplitude rapidly vanishes in azimuthal direction. This is even true for very low values of n. Peaking in both the azimuthal and radial direction becomes more pronounced for larger values of n. This tendency is presented in a more detailed fashion in Fig. 5. In the upper graph the radial half width, H_s, is plotted as a function of the growthrate squared, Γ^2, for different values of n. With increasing n, the half width decreases. A cross-plot of H_s as a function of $1/\sqrt{n}$ for different values of Γ^2 is shown in the lower graph of Fig. 5. It can be seen that H_s is proportional to $1/\sqrt{n}$ and approaches zero for $n \to \infty$.

The unstable region in which the potential energy density

$$W_p(s) = \int_0^{2\pi} d\chi \, W_p(s,\chi) \qquad (12)$$

is negative and proportional to $1/\sqrt{n}$ becomes narrower as q_0 increases. Figure 6 shows the radial domain in which $W_p(s) < 0$ as a func-

tion of q_0. The dashed curve has been calculated using a ballooning code for $n = \infty$ with which each s = constant surface is checked. For the calculations using finite but high n number, there are, in general, many unstable modes with different radial wavenumbers. What we present in Fig. 6 is the radial region for which $W_p < 0$ for the most unstable $n = 3$ and $n = 100$ modes. The "unstable" region of the most unstable $n = 100$ mode does not cover the whole $n = 100$ unstable ballooning region. There are other unstable $n = 100$ modes with lower growthrates which show negative potential energy densities at other radii. Increasing n increases the number of such unstable modes. The region where $W_p(s) < 0$ for $n = 3$ exceeds that of the ballooning theory for $n = \infty$. The width of this "unstable" region is almost independent of q_0. There are strong positive contributions to W_p near the axis and near the surface which nearly cancel the negative contributions. For $q_0 > 1.65$, the mode suddenly becomes stable.

4. WEAK BALLOONING MODES

Both the radial and the azimuthal localization of the mode structure are drastically different for the weak shear Solovev equilibrium. For the strong shear case, the amplitude of the mode almost vanishes inside the torus at $\chi = \pi$ (see Fig. 4a), whereas for the weak shear case, the amplitude oscillates radially (Fig. 7). The positions of the maxima of the oscillation correspond to the positions of singular surfaces. A similar oscillatory behaviour is exhibited in the graphs, for $n = 3$ and $n = 10$, of the potential energy density (Eq. 12) versus the radial coordinate, s (Fig. 8). The positive contributions to W_p are located around singular surfaces. Between singular sur-

faces are negative contributions. This is different to that observed for the strong shear case where only one region of negative $W_p(s)$ appeared. The square of the growthrate, Γ^2, depends on the number of singular surfaces in the plasma, as is shown in Fig. 9 where Γ^2 is presented as a function of a fractional n-number. Here, n plays the role of the continuous longitudinal wavenumber k in cylindrical geometry. In the high-n region, we have many singular surfaces in the plasma which results in a continuous increase in the value of $\Gamma^2(n)$ as n is increased. The more singular surfaces are near the plasma surface, the less the mode feels the boundary. For small values of n, however, the boundary is strongly felt by the mode and, as a consequence, an oscillatory behaviour of $\Gamma^2(n)$ is observed. The minima and maxima are related to the number of singular surfaces in the plasma (see Table 1). The maxima at n = 1.8 and 2.8 occur when there are 2 and 3 singular surfaces whereas minima at n = 2.1 and 3.1 appear when there are only 1 and 2 minima in the plasma. For low, integral values of n, it is possible, by an appropriate choice of q_0, to fall into the stability regions.

5. DISCUSSION AND CONCLUSIONS

By using the new ERATO code, which incorporates an extraction of the ballooning phase factor, we have been able to confirm numerically that the marginal points of the high n modes smoothly approach the prediction of ballooning theory. The width of the radial localization of the modes is proportional to $1/\sqrt{n}$ in the case of strong shear. For this case, the amplitude of the mode is smoothly varying in both the radial and azimuthal direction, and can be well represented by our

code for values of n up to 100 by accumulating the mesh cells properly. Including finite Larmor radius effects (Itoh and Itoh, 1981), one sees that ballooning theory gives pessimistic limits. The real β limit is found to be 20% higher than that predicted by classical ballooning theory. In the case of low shear, the modes are sensitive to the presence of the singular surfaces. Due to the oscillatory nature of the position of the singular surfaces, the growthrate and the marginal value of q_o oscillate when changing n continuously. We see that the radial structure of the amplitude is more pronounced than the azimuthal structure.

This work has been supported by the Ecole Polytechnique Fédérale de Lausanne, by the Swiss National Science Foundation and by Euratom.

REFERENCES

Berger D., Bernard L.C., Gruber R. and Troyon F. (1980) ZAMP 31, 113.

Charlton L.A., Nelson D.B. and Dory K.A. (1980) Nucl. Fusion 20, 339.

Connor J.W., Hastie R.J. and Taylor J.B. (1978) Phys. Rev. Lett. 40, 396.

Dewar R.L., Manickam J., Grimm R.C. and Chance M.S. (1981) Nucl. Fusion 21, 493.

Grimm R.C., Greene J.M. and Johnson J.L. (1975) Methods of Computational Physics, Vol. 16, Ch. 4, Academic Press.

Gruber R., Schreiber R., Troyon F., Kerner W., Lackner K., Sykes A. and Wesson J.A. (1979) Plasma Physics and Controlled Nuclear Fusion Research, Vol. 1, p. 593, IAEA.

Gruber R., Semenzato S., Troyon F., Tsunematsu T., Kerner W., Merkel P. and Schneider W. (1981b), Comp. Phys. Commun. 24, 363 (1981)

Gruber R., Troyon F., Berger D., Bernard L.C., Rousset S., Schreiber R., Kerner W., Schneider W. and Roberts K.V. (1981a) Comput. Phys. Commun. 21, 323.

References (cont'd)

Hastie R.J. and Taylor J.B. (1981) Nucl. Fusion 21, 187.

Itoh S.I. and Itoh K. (1981) Nucl. Fusion 21, 3.

Kerner W. (1976) Nucl. Fusion 16, 643.

Küppers G., Pfirsch D. and Tasso H. (1971) Plasma Physics and Controlled Nuclear Fusion Research, Vol. 2, p. 529, IAEA.

Rousset S., Gruber R. and Troyon F. (1979) ZAMP 30, 862.

Solovev L.S. (1968) Soviet Phys. JETP 26, 400.

Sykes A., Wesson J.A. and Cox S.J. (1977) Phys. Rev. Lett. 39, 757.

Sykes A., Turner M.F., Fielding P.J. and Haas F.A. (1979) Plasma Physics and Controlled Nuclear Fusion Research, Vol. 1, p. 625, IAEA.

Takeda T., Itoh K., Azumi M., Kurita G., Takizuka T., Tokuda S., Tsunematsu T., Tuda T., Itoh S.I., Matsuura T. and Tanaka Y., (1981) Japan. Atomic Energy Research Institute, JAERI-M 9466.

FIGURE CAPTIONS

Fig. 1 The coordinate system R_m is the radius of the magnetic axis.

Fig. 2 The profiles of the safety factor, q, for the strong shear case, W6, and the weak shear case, S1.

Fig. 3 Growthrate squared, Γ^2, as a function of q_0 for different toroidal wave numbers, n. The $n = \infty$ curve is determined by extrapolation. The dashed curve is the stability limit calculated when finite Lamor radius stabilization effects are included. All calculations are performed with 50 intervals in radial and azimuthal directions. The dot (•) at $q_0 = 2.4$ indicates the stability limit determined by ballooning mode theory for $n = \infty$.

Fig. 4 Azimuthal (a) and radial (b) structures of the amplitude of the symmetric normal component for different toroidal wave numbers.

Fig. 5 Radial half width as a function of the growthrate squared, Γ^2, (upper graph) and of the toroidal wave numbers (lower graph). The lower graph is a cross-plot of the upper one. Note that the extrapolated lines go through the axis ($n = \infty$, $H_s = 0$).

Figure Captions (cont'd)

Fig. 6 Radial domain in which the potential energy density, $W_p(s)$, is negative versus q_0. The dashed curve indicates the $n = \infty$ ballooning limit.

Fig. 7 Radial structure of the amplitude of the symmetric component outside ($\chi = 0$) and inside ($\chi = \pi$) the torus. The upper graph is for $n = 3$ and the lower for $n = 10$.

Fig. 8 Radial structure of the potential energy density, $W_p(s)$, for $n = 3$ (upper) and $n = 10$ (lower graph). The positive regions are located around the singular surfaces.

Fig. 9 Growthrates squared, Γ^2, as a function of continuous n variable for three different values of q_0. The oscillatory behaviour arises from the position of the singular surfaces.

Table 1:

Location of extrema of $\Gamma^2(n)$

n	n_{qo}	n_{qs}	Number of singular surfaces of the plasma	Γ^2
1.8	1.89	3.34	2	maximum
2.1	2.21	3.87	1	minimum
2.8	2.94	5.15	3	maximum
3.1	3.26	5.71	2	minimum

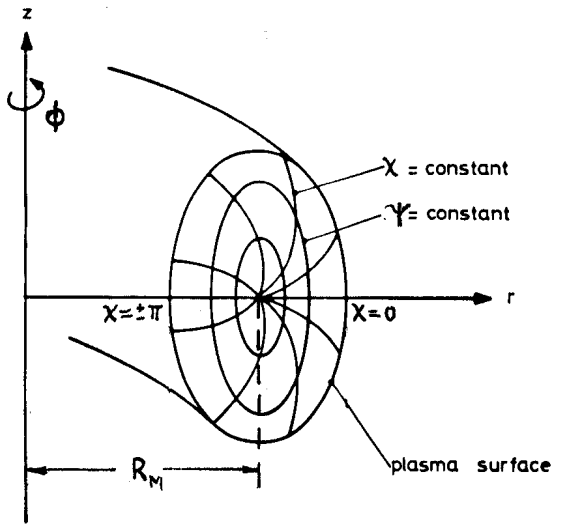

FIG. 1

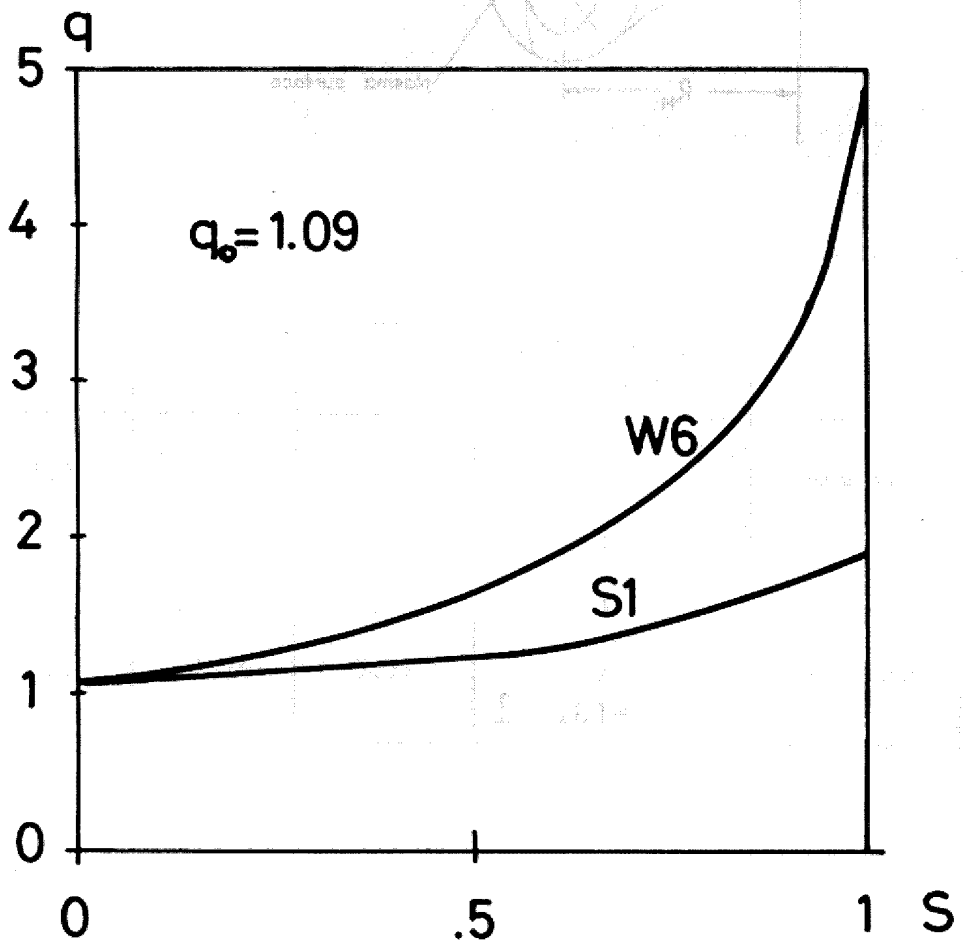

FIG. 2

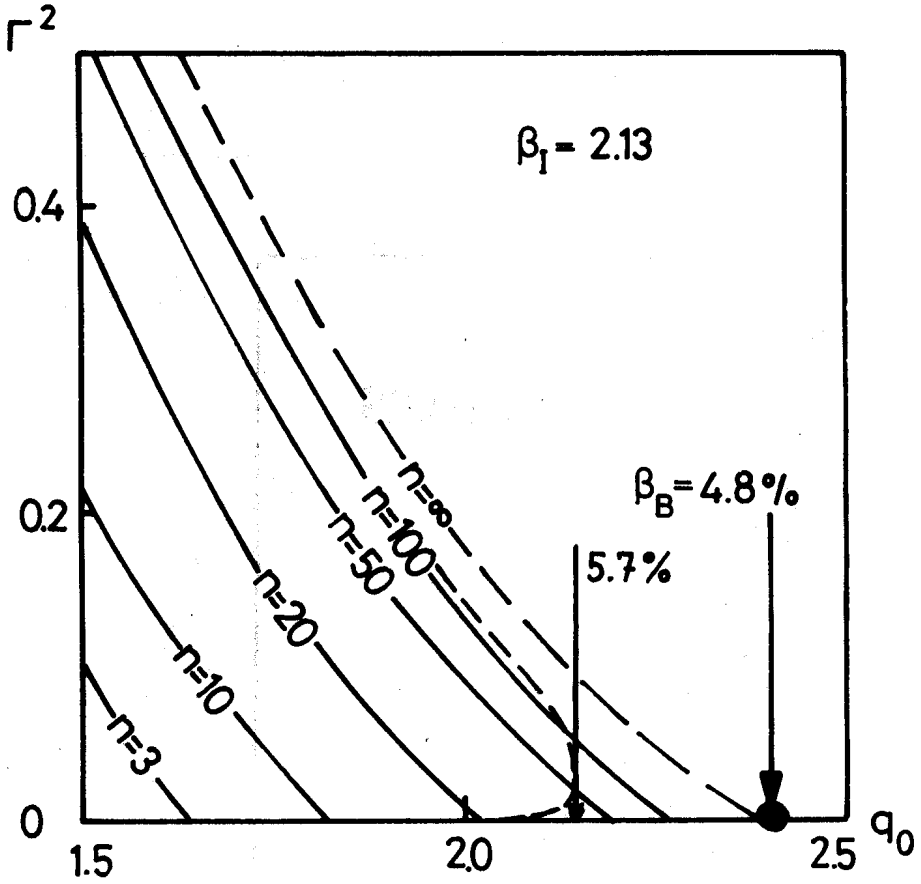
Γ^2
$\beta_I = 2.13$
0.4
0.2
0
n=∞
n=100
n=50
n=20
n=10
n=3
$\beta_B = 4.8\%$
5.7%
1.5
2.0
2.5
q_0

FIG. 3

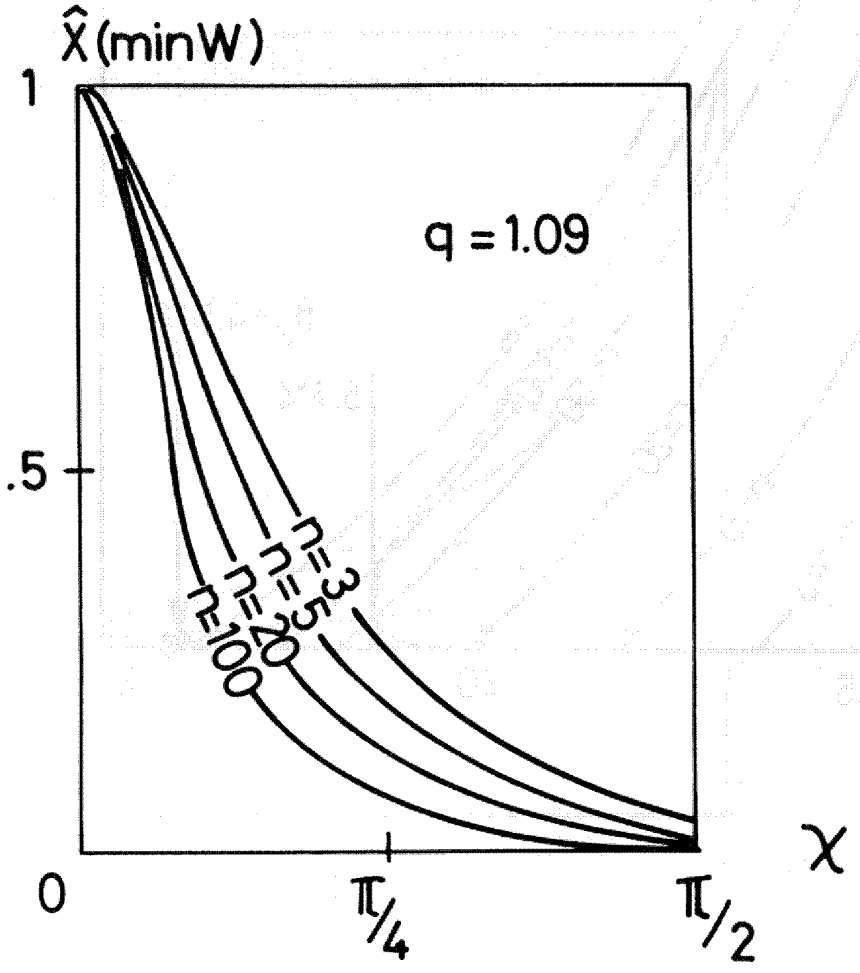

FIG. 4A

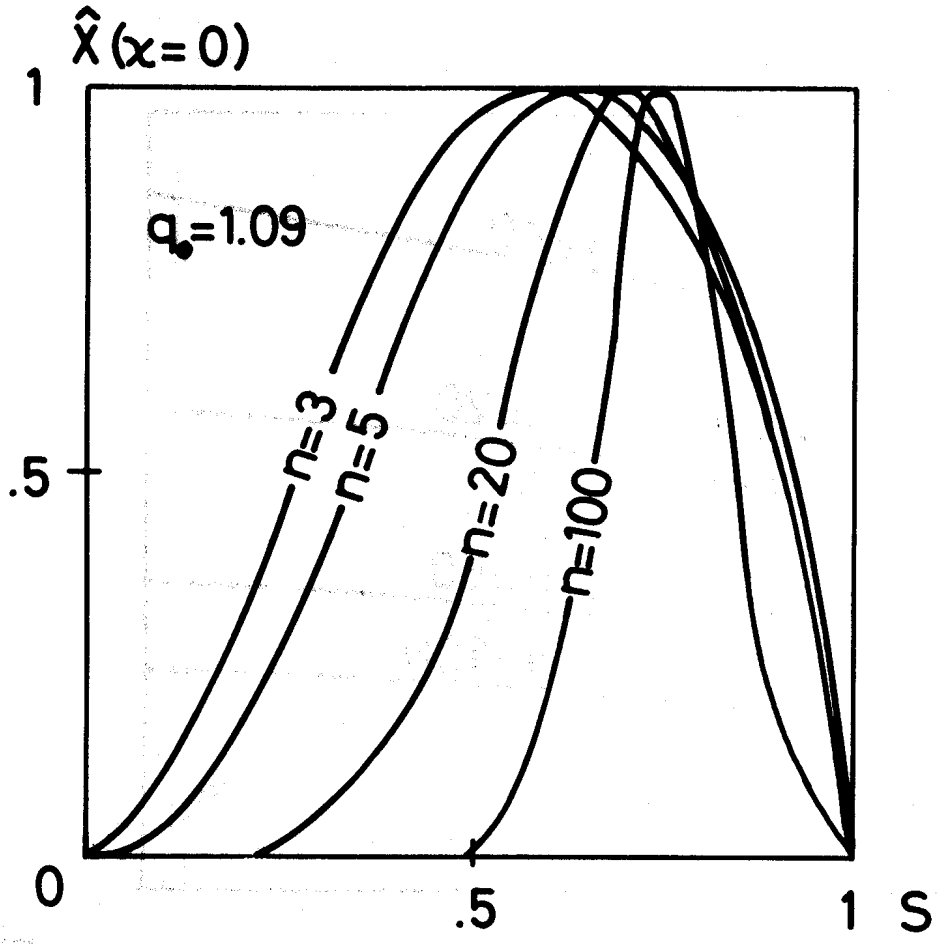

FIG. 4 B

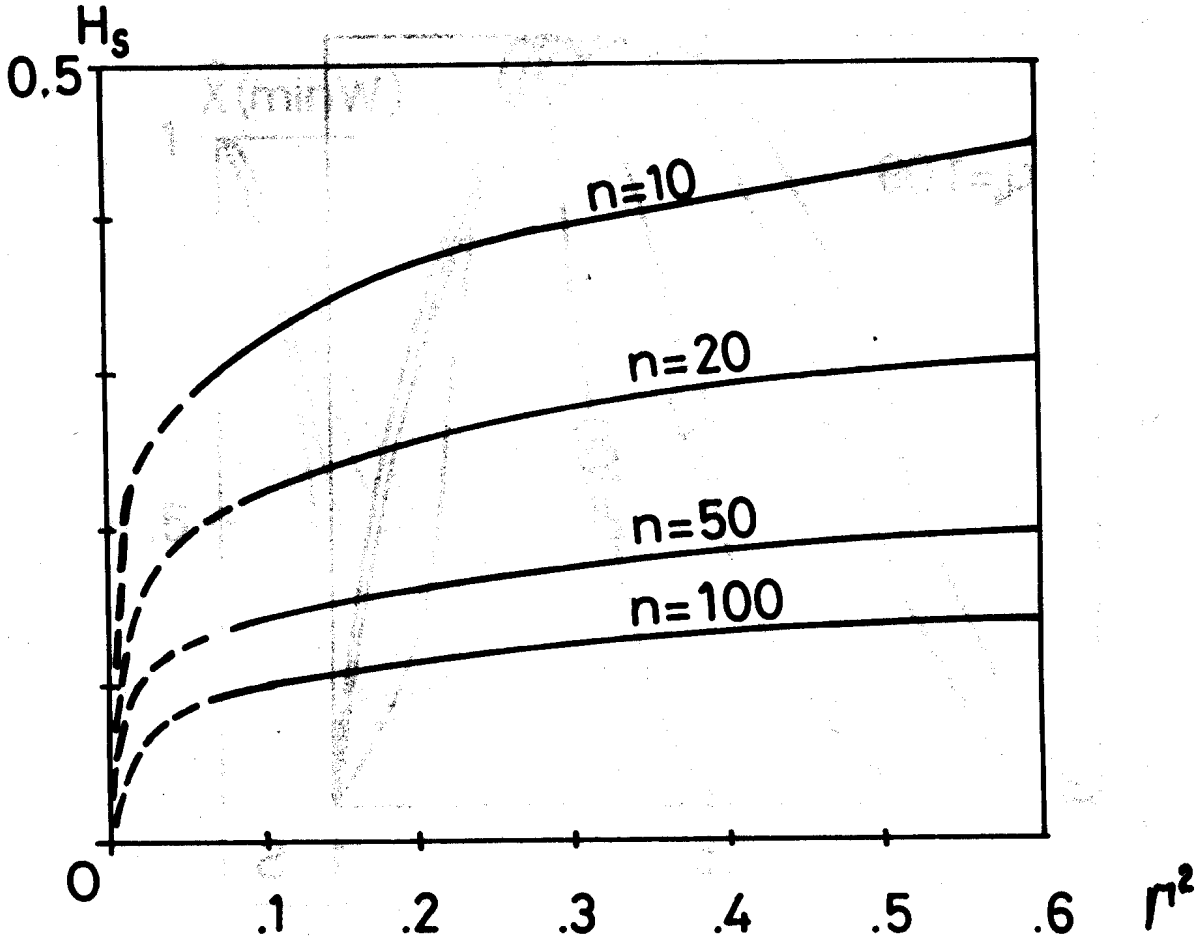

FIG. 5 UPPER

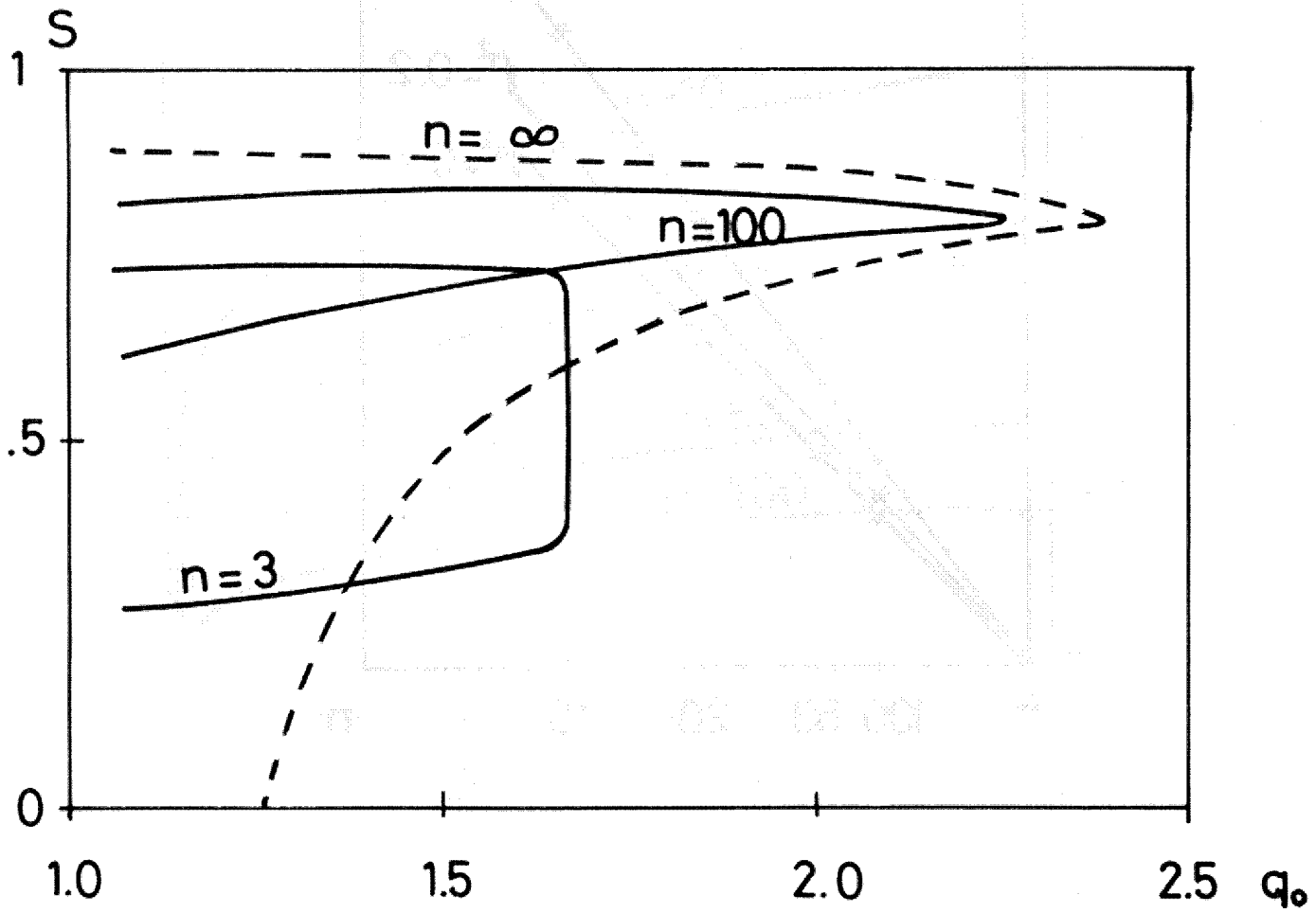

FIG. 6

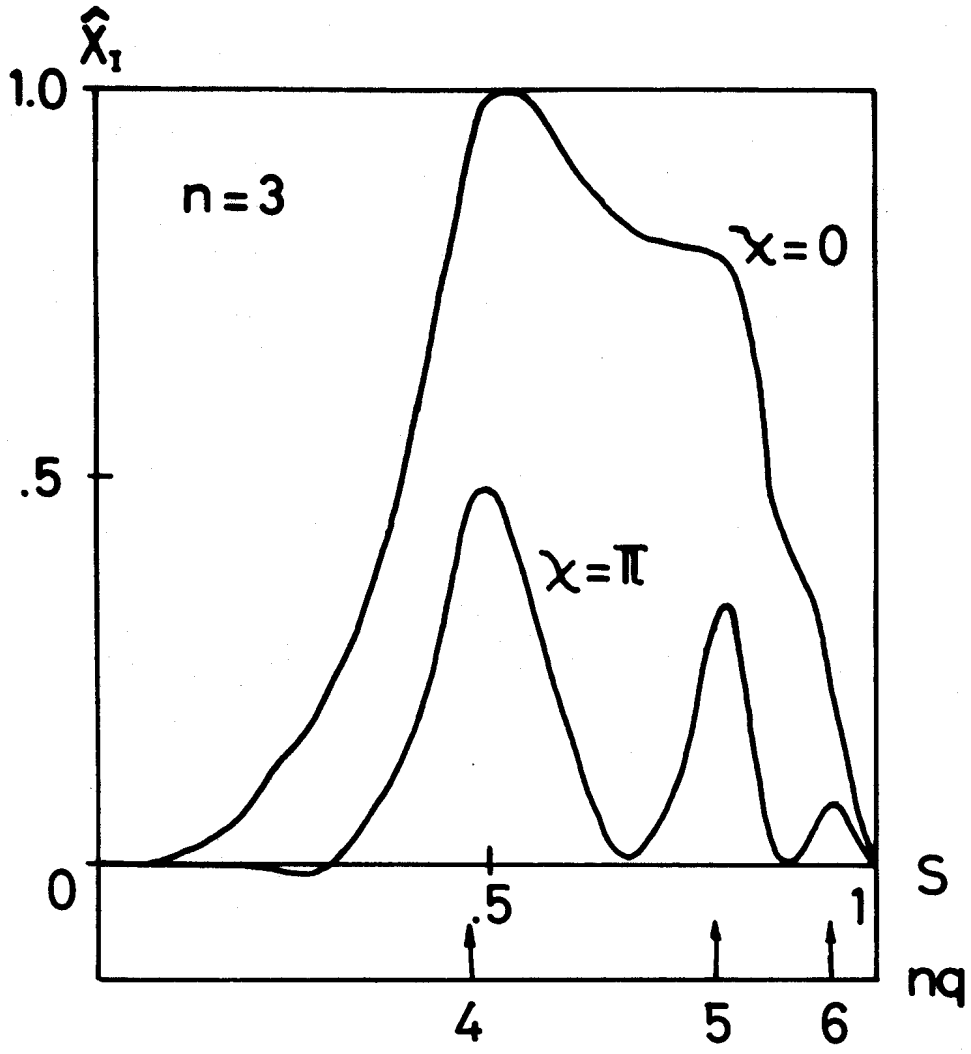
$\hat{\chi}_I$
1.0
.5
0
n = 3
$\chi = 0$
$\chi = \pi$
.5
1
S
4
5
6
nq

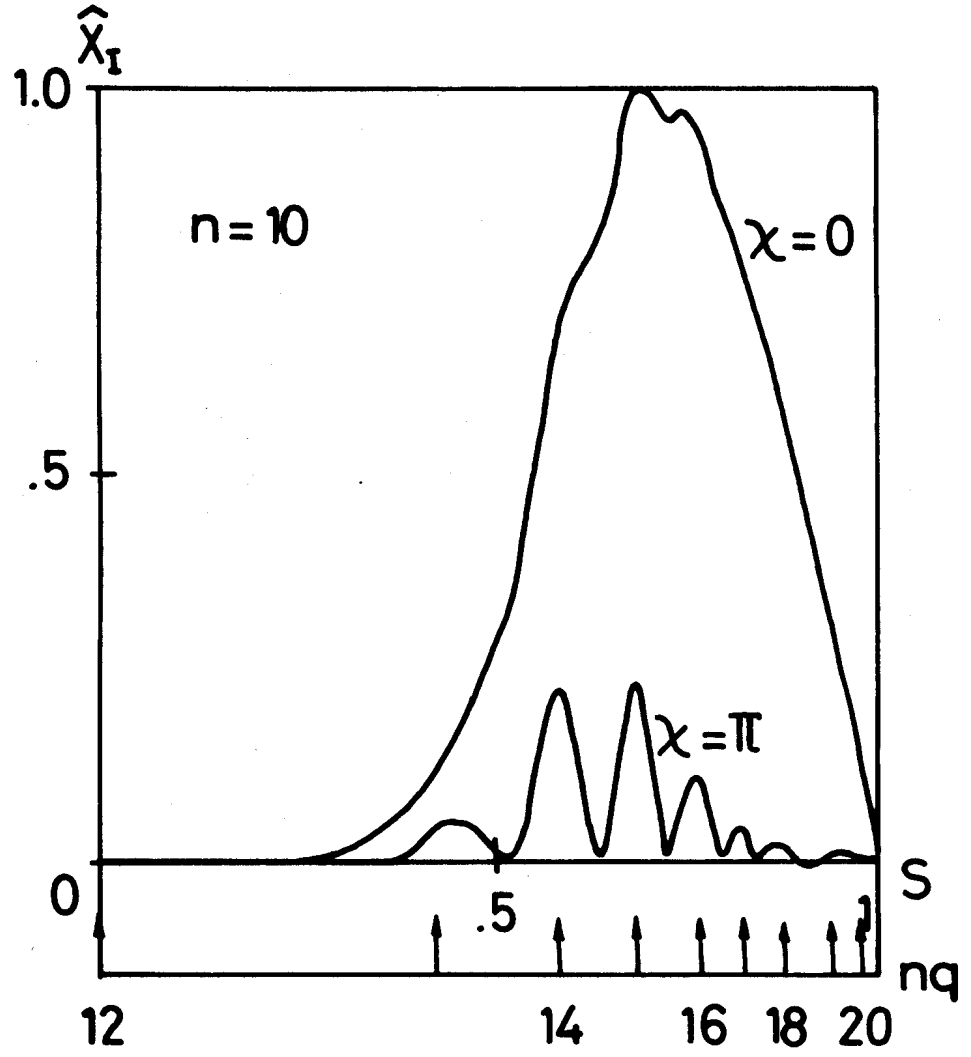
$\hat{\chi}_I$
1.0
.5
0
n = 10
$\chi = 0$
$\chi = \pi$
.5
1
S
12
14
16
18
20
nq

FIG. 7

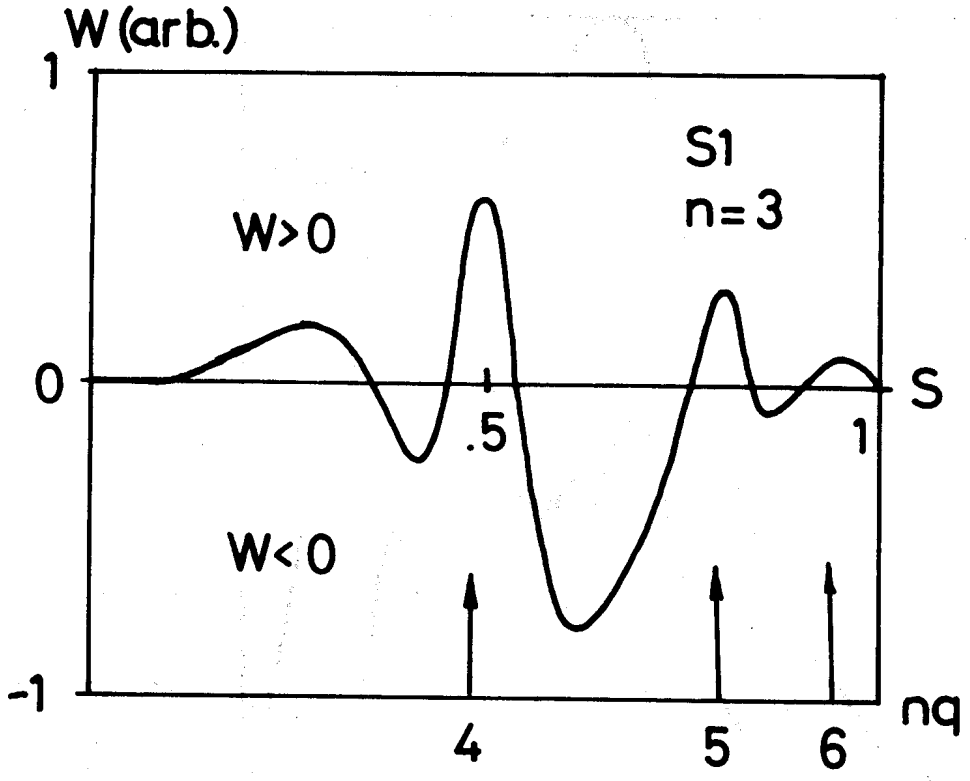
W(arb.)
1
S1
n=3
W>0
0
S
.5
1
W<0
-1
4
5
6
nq

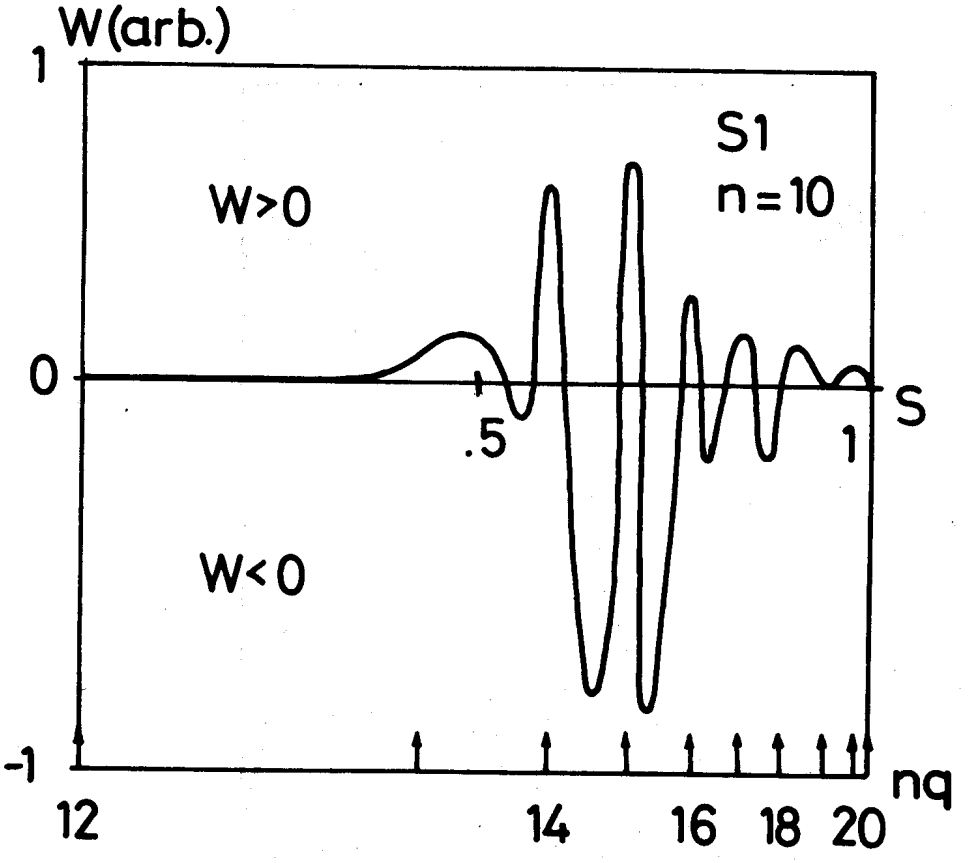
W(arb.)
1
S1
n=10
W>0
0
S
.5
1
W<0
-1
12
14
16
18
20
nq

FIG. 8